Dirac and Majorana edge states in graphene and topological superconductors

Akhmerov, A.R.

Chapter 1

Introduction

The two parts of this thesis: "Dirac edge states in graphene" and "Majorana edge states in topological superconductors" may seem very loosely connected to the reader. To study the edges of graphene, a one-dimensional sheet of carbon, one needs to pay close attention to the graphene lattice and accurately account for the microscopic details of the system. The Majorana fermions, particles which are their own anti-particles, are on the contrary insensitive to any perturbation and possess universal properties which are insensitive to microscopic details.

Curiously, the history of graphene has parallels with that of Majorana fermions. Graphene was first analysed in 1947 by Wallace [1], and the term "graphene" was invented in 1962 by Boehm and co-authors [2]. However, it was not until 2005, after graphene was synthesized in the group of Geim [3], that there appeared an explosion of research activity, culminating in the Nobel prize five years later. Majorana fermions were likewise described for the first time a long time ago, in 1932 [4], and then were mostly forgotten until the interest in them revived in high energy physics decades later. For the condensed matter physics community Majorana fermions acquired an important role only in the last few years, when they were predicted to appear in several condensed matter systems [5–7], and to provide a building block for a topological quantum computer [8, 9].

There are two other more relevant similarities between edge states in graphene and in topological superconductors. To understand what they are, we need to answer the question "what is special about the edge states in these systems?" Edge states in general have been known for a long time [10, 11] — they are electronic states localized at the interface of a material with vacuum or another material. They may or may not appear, and their presence depends sensitively on microscopic details of the interface.

The distinctive feature of the edge states studied here is that they are protected by a certain physical symmetry of the system. This protection by symmetry ensures that they always exist at a fixed energy: at the Dirac point in graphene and at the Fermi energy in topological superconductors. Additionally, protection by symmetry ensures that the edge states possess universal properties — they occur at a large set of boundaries, and their presence can be deduced from the bulk properties.

Another property shared by graphene and topological superconductors is that both are well described by the Dirac equation, as opposed to the Schrödinger equation suitable for most other condensed matter systems. This is in no respect accidental and is tightly related to the symmetry properties of the two systems. In graphene the symmetry ensuring the presence of the edge states is the so-called sublattice symmetry. Using only this symmetry one may derive that graphene obeys the Dirac equation on long length scales. The appearance of the Dirac equation in topological superconductors is also natural, once one realizes that the phase transition into a topologically nontrivial state is scale invariant, and that the Dirac Hamiltonian is one of the simplest scale-invariant Hamiltonians.

An understanding of the role of symmetry in the study of edge states and familiarity with the Dirac equation are necessary and sufficient to understand most of this thesis. In this introductory chapter we describe both and explain how they apply to graphene and topological superconductors.

1.1 Role of symmetry in the protection of edge states

The concept of symmetry plays a central role in physics. It is so influential because complete theories may be constructed by just properly taking into account the relevant symmetries. For example, electrodynamics is built on gauge symmetry and Lorentz symmetry. In condensed matter systems there are only three discrete symmetries which survive the presence of disorder: time-reversal symmetry (denoted as $\mathcal{T}$), particle-hole symmetry (denoted as $\mathcal{CT}$), and sublattice or chiral symmetry (denoted as $\mathcal{C}$). The time-reversal symmetry and the particle-hole symmetry have anti-unitary operators. These may square either to $+1$ or -1 depending on the spin of particles and on spin-rotation symmetry being present or absent. Chiral symmetry has a unitary operator and always squares to $+1$. Together these three symmetries form ten symmetry classes [12], each class characterized by the type (or absence of) time-reversal and particle-hole symmetry and the possible presence of chiral symmetry.

Sublattice symmetry and particle-hole symmetry require that for every eigenstate $|\psi\rangle$ of the Hamiltonian H with energy ε there is an eigenstate of the same Hamiltonian given by either $\mathcal{C}|\psi\rangle$ or $\mathcal{CT}|\psi\rangle$ with energy $-\varepsilon$. We observe that eigenstates of the Hamiltonian with energy $\varepsilon = 0$ are special in that they may transform into themselves under the symmetry transformation. Time-reversal symmetry implies no such property, and hence is unimportant for what follows. We proceed to discuss in more detail what is the physical meaning of sublattice and particle-hole symmetries and of the zero energy states protected by them.

1.1.1 Sublattice symmetry

Let us consider a set of atoms which one can split into two groups, such that the Hamiltonian contains only matrix elements between the two groups, but not within the same

group. This means that the system of tight-binding equations describing the system is

$$\varepsilon\psi_i^A = \sum t_{ij}\psi_j^B, \tag{1.1a}$$

$$\varepsilon\psi_i^B = \sum t_{ij}\psi_j^A, \tag{1.1b}$$

where we call one group of atoms sublattice A, and another group of atoms sublattice B. Examples of bipartite lattices are shown in Fig. 1.1, with the panel a) showing the honeycomb lattice of graphene.

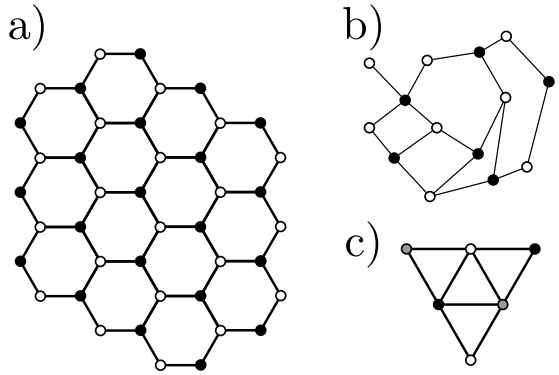

Figure 1.1: Panel a): the bipartite honeycomb lattice of graphene. Panel b): an irregular bipartite lattice. Panel c): an example of a lattice without bipartition. Nodes belonging to one sublattice are marked with open circles, nodes belonging to the other one by black circles, and finally nodes which belong to neither of the sublattices are marked with grey circles.

The Hamiltonian of a system with chiral symmetry can always be brought to a form

$$H = \begin{pmatrix} 0 & T \\ T^\dagger & 0 \end{pmatrix}, \tag{1.2}$$

with T the matrix of hopping amplitudes from one sublattice to another. Now we are ready to construct the chiral symmetry operator. The system of tight-binding equations stays invariant under the transformation $\psi^B \to -\psi^B$ and $\varepsilon \to -\varepsilon$. In terms of the Hamiltonian this translates into a symmetry relation

$$\mathcal{C}H\mathcal{C} = -H, \tag{1.3}$$

$$\mathcal{C} = \mathrm{diag}(1, 1, \ldots, 1, -1, \ldots, -1). \tag{1.4}$$

The number of 1's and -1's in $\mathcal{C}$ is equal to the number of atoms in sublattices A and B respectively.

Let us now consider a situation when the matrix T has vanishing eigenvalues, or in other words when we are able to find $|\psi^A\rangle$ such that $T|\psi^A\rangle = 0$. This means that

$(\psi^A, 0)$ is a zero energy eigenstate of the full Hamiltonian. Moreover since the diagonal terms in the Hamiltonian are prohibited by the symmetry, this eigenstate can only be removed from zero energy by coupling it with an eigenstate which belongs completely to sublattice B. If sublattice A has N more atoms than sublattice B, this means that the matrix T is non-square and always has exactly N more zero eigenstates than the matrix $T^\dagger$. Hence there will be at least N zero energy eigenstates in the system, a result also known as Lieb's theorem [13].

Analogously, if there are several modes localized close to a single edge, they cannot be removed from zero energy as long as they all belong to the same sublattice. One of the central results presented in this thesis is that this is generically the case for a graphene boundary.

1.1.2 Particle-hole symmetry

On the mean-field level superconductors are described by the Bogoliubov-de-Gennes Hamiltonian [14]

$$H_{\text{BdG}} = \begin{pmatrix} H_0 - E_F & \Delta \\ \Delta^\dagger & E_F - \mathcal{T}^{-1} H_0 \mathcal{T} \end{pmatrix}, \tag{1.5}$$

with H_0 the single-particle Hamiltonian, E_F the Fermi energy, and Δ the pairing term. This Hamiltonian acts on a two-component wave function $\psi_{\text{BdG}} = (u, v)^T$ with u the particle component of the wave function and v the hole component. The many-body operators creating excitations above the ground state of this Hamiltonian are $\gamma^\dagger \equiv uc^\dagger + vc$, with $c^\dagger$ and c electron creation and annihilation operators.

This description is redundant; for each eigenstate $\psi_\varepsilon = (u_0, v_0)^T$ of H_{BdG} with energy ε there is another eigenstate $\psi_{-\varepsilon} = (\mathcal{T} v_0, -\mathcal{T} u_0)^T$. The redundancy is manifested in the fact that the creation operator $\gamma^\dagger$ of the quasiparticle in the ψ_ε state is identical to the annihilation operator γ of the quasiparticle in the $\psi_{-\varepsilon}$ state. In other words, the two wave functions ψ_ε and $\psi_{-\varepsilon}$ correspond to a single quasiparticle, and the creation of a quasiparticle with positive energy is identical to the annihilation of a quasiparticle with negative energy. The origin of the redundancy lies in the doubling of the degrees of freedom [15], which has to be applied to bring the many-body Hamiltonian to the non-interacting form (1.5). For the Hamiltonian H_{BdG} this $\mathcal{CT}$ symmetry is expressed by the relation

$$(i\tau_y \mathcal{T})^{-1} H_{\text{BdG}} (i\tau_y \mathcal{T}) = -H_{\text{BdG}}, \tag{1.6}$$

where τ_y is the second Pauli matrix in the electron-hole space.

Let us now study what happens if there is an eigenstate of H_{BdG} with exactly zero energy, similar to the way we studied the case of the sublattice-symmetric Hamiltonian. This eigenstate transforms into itself after applying $\mathcal{CT}$ symmetry: $\psi_0 = \mathcal{CT}\psi_0$, hence it has to have a creation operator $\gamma^\dagger$ which is equal to the annihilation operator γ of its electron-hole partner.

Let us now, similar to the case of sublattice symmetry, study what happens if there is an eigenstate of H_{BdG} with exactly zero energy which transforms into itself after applying $\mathcal{CT}$ symmetry: $\psi_0 = \mathcal{CT}\psi_0$. This state has to have a creation operator $\gamma^\dagger$

which is equal to the annihilation operator γ of its electron-hole partner. Since this state is an electron-hole partner of itself, we arrive to $\gamma^\dagger = \gamma$. Fermionic operators which satisfy this property are called *Majorana fermions*. Just using the defining properties we can derive many properties of Majorana fermions. For example let us calculate the occupation number $\gamma^\dagger\gamma$ of a Majorana state. We use the fermionic anticommutation relation

$$\gamma^\dagger\gamma + \gamma\gamma^\dagger = 1. \tag{1.7}$$

Then, by using the Majorana condition, we get $\gamma\gamma^\dagger = \gamma^2 = \gamma^\dagger\gamma$. After substituting this into the anticommutation relation we immediately get $\gamma^\dagger\gamma = 1/2$. In other words, any Majorana state is always half-occupied.

Unlike the zero energy states in sublattice-symmetric systems, which shift in energy if an electric field is applied because the sublattice symmetry is broken, a Majorana fermion can only be moved away from zero energy by being paired with another Majorana fermion, because every state at positive energy has to have a counterpart at negative energy.

1.2 Dirac Hamiltonian

The Dirac equation was originally conceived to settle a disagreement between quantum mechanics and the special theory of relativity, namely to make the Schrödinger equation invariant under Lorentz transformation. The equation in its original form reads

$$i\hbar\frac{d\psi}{dt} = \left(\sum_{i=1}^{3}\alpha_i p_i c + \beta mc^2\right)\psi. \tag{1.8}$$

Here β and α_i form a set of 4×4 Dirac matrices, m and p_i are mass and momentum of the particle, and c is the speed of light. For $p \ll mc$ the spectrum of this equation is conical, and it has a gap between $+m$ and $-m$.

In condensed matter physics the term Dirac equation is used more loosely for any Hamiltonian which is linear in momentum:

$$H = \sum_i \alpha_i p_i v_i + \sum_j m_j \beta_j. \tag{1.9}$$

In such a case m_j are called mass terms and v_i velocities. The set of Hermitian matrices α_i, β_i do not have to satisfy the anticommutation relations, unlike the original Dirac matrices. The number of components of the wave function also does not have to be equal to 4: it is even customary to call $H = vp$ a Dirac equation. The symmetry properties of these equations are fully determined by the set of matrices α_i, β_i, making the Dirac equation a very flexible tool in modeling different physical systems. Since the spectrum of the Dirac equation is unbounded both at large positive and large negative energies, this equation is an effective low-energy model.

In this section we focus on two contexts in which the Dirac equation appears: it occurs typically in systems with sublattice symmetry and in particular in graphene; also it allows to study topological phase transitions in insulators and superconductors.

1.2.1 Derivation of Dirac Hamiltonian using sublattice symmetry and its application to graphene

To derive a dispersion relation of a system with sublattice symmetry, we start from the Hamiltonian (1.2). After transforming it to momentum space by applying Bloch's theorem, we get the following Hamiltonian:

$$H = \begin{pmatrix} 0 & Q(\boldsymbol{k}) \\ Q^{\dagger}(\boldsymbol{k}) & 0 \end{pmatrix}, \tag{1.10}$$

where Q is a matrix which depends on the two-dimensional momentum $\boldsymbol{k}$. Let us now consider a situation when the phase of $\det Q(\boldsymbol{k})$ winds around a unit circle as k goes around a contour Γ in momentum space. Since $\det Q(\boldsymbol{k})$ is a continuous complex function, it has to vanish in a certain point $\boldsymbol{k_0}$ inside this contour. Generically a single eigenvalue of Q vanishes at this point. Since we are interested in the low energy excitation spectrum, let us disregard all the eigenvectors of Q which correspond to the non-vanishing eigenvalues and expand $Q(\boldsymbol{k})$ close to the momentum where it vanishes:

$$Q = v_x \delta k_x + v_y \delta k_y + \mathcal{O}(|\delta k^2|), \tag{1.11}$$

with v_x and v_y complex numbers, and $\boldsymbol{\delta k} \equiv \boldsymbol{k} - \boldsymbol{k_0}$. For Q to vanish only at $\delta k = 0$, $v_x v_y^*$ has to have a finite imaginary part. In that case the spectrum of the Hamiltonian assumes the shape of a cone close to $\boldsymbol{k_0}$, and the Hamiltonian itself has the form

$$H = |v_x|\delta k_x \begin{pmatrix} 0 & e^{i\alpha_x} \\ e^{-i\alpha_x} & \end{pmatrix} + |v_y|\delta k_y \begin{pmatrix} 0 & e^{i\alpha_y} \\ e^{-i\alpha_y} & \end{pmatrix}, \quad \alpha_x \neq \alpha_y. \tag{1.12}$$

We see that the system is indeed described by a Dirac equation with no mass terms. The point $\boldsymbol{k_0}$ in the Brillouin zone is called a Dirac point. Since the winding of $\det Q(\boldsymbol{k})$ around the border of the Brillouin zone must vanish, we conclude that there should be as many Dirac points with positive winding around them, as there are with negative winding. In other words the Dirac points must come in pairs with opposite winding. If in addition time-reversal symmetry is present, then $Q(\boldsymbol{k}) = Q^*(-\boldsymbol{k})$, and the Dirac points with opposite winding are located at opposite momenta.

We are now ready to apply this derivation to graphene. Since there is only one atom of each sublattice per unit cell (as shown in Fig. 1.2), $Q(\boldsymbol{k})$ is a number rather than a matrix. The explicit expression for Q is

$$Q = e^{i\boldsymbol{k}\cdot\boldsymbol{a}_1} + e^{i\boldsymbol{k}\cdot\boldsymbol{a}_2} + e^{i\boldsymbol{k}\cdot\boldsymbol{a}_3}, \tag{1.13}$$

with vectors $\boldsymbol{a}_1, \boldsymbol{a}_2, \boldsymbol{a}_3$ shown in Fig. 1.2. It is straightforward to verify that Q vanishes at momenta $(\pm 4\pi/3a, 0)$. These two momenta are called K and K' valleys of the dispersion respectively. The Dirac dispersion near each valley has to satisfy the three-fold rotation symmetry of the lattice, which leads to $v_x = i v_y$. Further, due to the mirror symmetry around the x-axis, v_x has to be real, so we get the Hamiltonian

$$H = v \begin{pmatrix} \sigma_x p_x + \sigma_y p_y & 0 \\ 0 & \sigma_x p_y - \sigma_y p_y \end{pmatrix}, \tag{1.14}$$

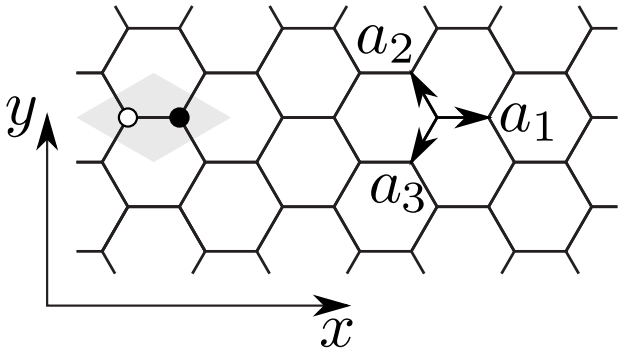

Figure 1.2: Lattice structure of graphene. The grey rhombus is the unit cell, with sublattices A and B marked with open and filled circles respectively.

where the matrices σ_i are Pauli matrices in the sublattice space. The first two components of the wave function in this 4-component equation correspond to the valley K, and the second two to the valley $K^{'}$. We will find it convenient to perform a change of basis $H \to UHU^{\dagger}$ with $U = \mathrm{diag}(\sigma_0, \sigma_x)$. This transformation brings the Hamiltonian to the valley-isotropic form:

$$H^{'} = v \begin{pmatrix} \sigma_x p_x + \sigma_y p_y & 0 \\ 0 & \sigma_x p_y + \sigma_y p_y \end{pmatrix}. \tag{1.15}$$

1.2.2 Dirac Hamiltonian close to a phase transition point

Let us consider the one-dimensional Dirac Hamiltonian

$$H = -i\hbar v \sigma_z \frac{\partial}{\partial x} + m(x)\sigma_y. \tag{1.16}$$

The symmetry $H^* = -H$ expresses particle-hole symmetry.[1] We search for eigenstates $\psi(x)$ of this Hamiltonian at exactly zero energy. Expressing the derivative of the wave function through the other terms gives

$$\frac{\partial \psi}{\partial x} = \frac{m(x)}{\hbar v}\sigma_x \psi. \tag{1.17}$$

The solutions of this equation have the form

$$\psi(x) = \exp\left(\sigma_x \int_{x_0}^{x} \frac{m(x^{'})dx^{'}}{\hbar v})\right)\psi(x_0). \tag{1.18}$$

[1] Any particle-hole symmetry operator of systems without spin rotation invariance can be brought to this form by a basis transformation.

There is only one Pauli matrix entering the expression, so the two linearly-independent solutions are given by

$$\psi_{\pm} = \exp\left(\pm \int_{x_0}^{x} \frac{m(x')dx'}{\hbar v}\right)\begin{pmatrix}1\\ \pm 1\end{pmatrix}. \tag{1.19}$$

At most one of the solutions is normalizable, and it is only possible to find a solution if the mass has opposite signs at $x \to \pm\infty$. In other words a solution exists if and only if there is a domain wall in the mass. The state bound at the interface between positive and negative masses is a Majorana bound state. The wave function corresponding to the Majorana state may change depending on the particular form of the function $m(x)$, but the presence or absence of the Majorana bound state is determined solely by the fact that the mass is positive on one side and negative on the other. An example of a domain wall in the mass and the Majorana bound state localized at the domain wall are shown in Fig. 1.3.

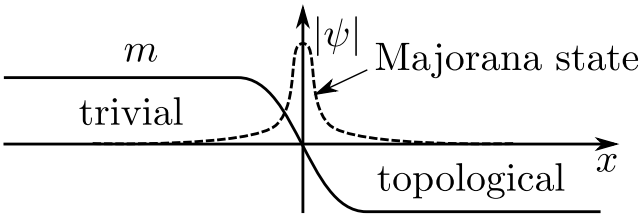

Figure 1.3: A model system with a domain wall in the mass. The domain with positive mass is called topologically trivial, the domain with negative mass is called topologically nontrivial. A Majorana bound state is located at the interface between the two domains.

The property that two domains with opposite mass have a symmetry-protected state at the interface, irrespective of the details of the interface, is called topological protection. Materials with symmetry-protected edge states are called topological insulators and superconductors. By selecting different mass terms in the Dirac equation one can change the symmetry class of the topological insulators or superconductors [16].

1.3 This thesis

We give a brief description of the content of each of the chapters.

1.3.1 Part I: Dirac edge states in graphene

Chapter 2: Boundary conditions for Dirac fermions on a terminated honeycomb lattice

We derive the boundary condition for the Dirac equation corresponding to a tight-binding model of graphene terminated along an arbitary direction. Zigzag boundary conditions

result generically once the boundary is not parallel to the bonds, as shown in Fig. 1.4. Since a honeycomb strip with zigzag edges is gapless, this implies that confinement by lattice termination does not in general produce an insulating nanoribbon. We consider the opening of a gap in a graphene nanoribbon by a staggered potential at the edge and derive the corresponding boundary condition for the Dirac equation. We analyze the edge states in a nanoribbon for arbitrary boundary conditions and identify a class of propagating edge states that complement the known localized edge states at a zigzag boundary.

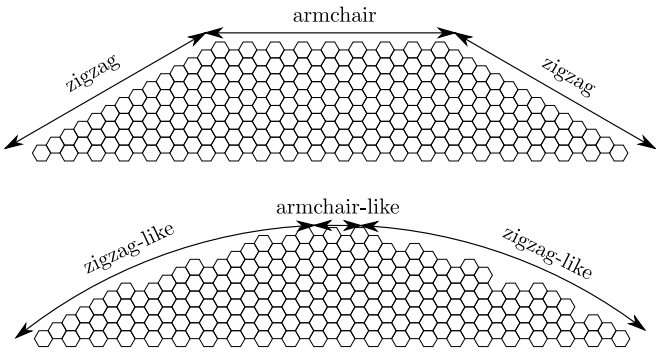

Figure 1.4: Top panel: two graphene boundaries appearing when graphene is terminated along one of the main crystallographic directions are the armchair boundary and the zigzag boundary. Only the zigzag boundary supports edge states. Bottom panel: when graphene is terminated along an arbitrary direction, the boundary condition generically corresponds to a zigzag one, except for special angles.

Chapter 3: Detection of valley polarization in graphene by a superconducting contact

Because the valleys in the band structure of graphene are related by time-reversal symmetry, electrons from one valley are reflected as holes from the other valley at the junction with a superconductor. We show how this Andreev reflection can be used to detect the valley polarization of edge states produced by a magnetic field using the setup of Fig. 1.5. In the absence of intervalley relaxation, the conductance $G_{NS} = 2(e^2/h)(1 - \cos\Theta)$ of the junction on the lowest quantum Hall plateau is entirely determined by the angle Θ between the valley isospins of the edge states approaching and leaving the superconductor. If the superconductor covers a single edge, $\Theta = 0$ and no current can enter the superconductor. A measurement of G_{NS} then determines the intervalley relaxation time.

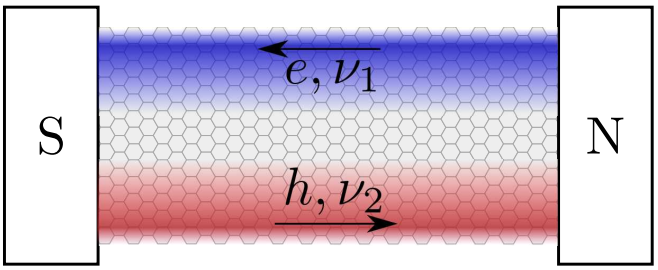

Figure 1.5: A normal metal-graphene-superconductor junction in high magnetic field. The only possibility for electric conductance is via the edge states. The valley polarizations ν_1, ν_2 of the edge states at different boundaries are determined only by the corresponding boundary conditions. The probability for an electron to reflect from the superconductor as a hole, as shown, depends on both ν_1 and ν_2.

Chapter 4: Theory of the valley-valve effect in graphene

A potential step in a graphene nanoribbon with zigzag edges is shown to be an intrinsic source of intervalley scattering – no matter how smooth the step is on the scale of the lattice constant a. The valleys are coupled by a pair of localized states at the opposite edges, which act as an attractor/repellor for edge states propagating in valley K/K'. The relative displacement Δ along the ribbon of the localized states determines the conductance G. Our result $G = (e^2/h)[1 - \cos(N\pi + 2\pi\Delta/3a)]$ explains why the "valley-valve" effect (the blocking of the current by a p-n junction) depends on the parity of the number N of carbon atoms across the ribbon, as shown in Fig. 1.6.

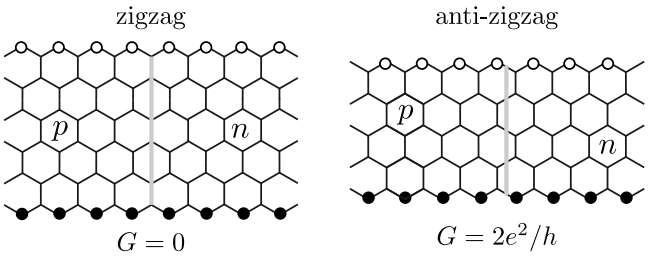

Figure 1.6: A pn-junction in zigzag and antizigzag ribbons (shown as a grey line separating p-type and n-type regions). The two ribbons are described on long length scales by the same Dirac equation, with the same boundary condition, however one ribbon is fully insulating, while the other one is perfectly conducting.

Chapter 5: Robustness of edge states in graphene quantum dots

We analyze the single particle states at the edges of disordered graphene quantum dots. We show that generic graphene quantum dots support a number of edge states proportional to the circumference of the dot divided by the lattice constant. The density of these edge states is shown in Fig. 1.7. Our analytical theory agrees well with numerical simulations. Perturbations breaking sublattice symmetry, like next-nearest neighbor hopping or edge impurities, shift the edge states away from zero energy but do not change their total amount. We discuss the possibility of detecting the edge states in an antidot array and provide an upper bound on the magnetic moment of a graphene dot.

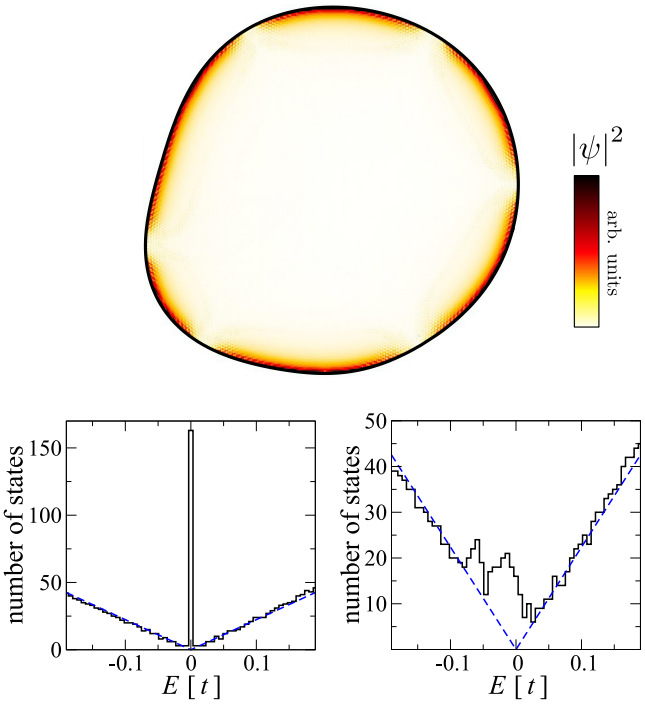

Figure 1.7: Density of low energy states in a graphene quantum dot as a function of position (top panel) or energy (bottom panels). The bottom left panel corresponds to the case when sublattice symmetry is present and the edge states are pinned to zero energy, while the bottom right panel shows the effect of sublattice symmetry breaking perturbations on the density of states.

1.3.2 Part II: Majorana bound states in topological superconductors

Chapter 6: Topological quantum computation away from ground state with Majorana fermions

We relax one of the requirements for topological quantum computation with Majorana fermions. Topological quantum computation was discussed so far as the manipulation of the wave function within a degenerate many-body ground state. Majorana fermions, are the simplest particles providing a degenerate ground state (non-abelian anyons). They often coexist with extremely low energy excitations (see Fig. 1.8), so keeping the system in the ground state may be hard. We show that the topological protection extends to the excited states, as long as the Majorana fermions interact neither directly, nor via the excited states. This protection relies on the fermion parity conservation, and so it is generic to any implementation of Majorana fermions.

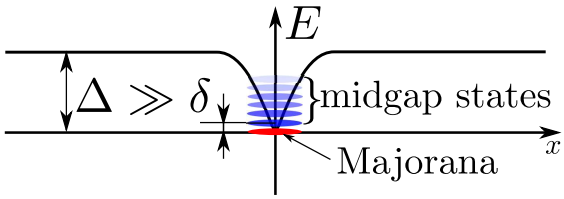

Figure 1.8: A Majorana fermion (red ellipse) coexists with many localized finite energy fermion states (blue ellipses) separated by a minigap δ, which is much smaller than the bulk gap Δ.

Chapter 7: Splitting of a Cooper pair by a pair of Majorana bound states

A single qubit can be encoded nonlocally in a pair of spatially separated Majorana bound states. Such Majorana qubits are in demand as building blocks of a topological quantum computer, but direct experimental tests of the nonlocality remain elusive. In this chapter we propose a method to probe the nonlocality by means of crossed Andreev reflection, which is the injection of an electron into one bound state followed by the emission of a hole by the other bound state (equivalent to the splitting of a Cooper pair over the two states). The setup we use is shown in Fig. 1.9. We have found that, at sufficiently low excitation energies, this nonlocal scattering process dominates over local Andreev reflection involving a single bound state. As a consequence, the low-temperature and low-frequency fluctuations δI_i of currents into the two bound states $i = 1, 2$ are maximally correlated: $\overline{\delta I_1 \delta I_2} = \overline{\delta I_i^2}$.

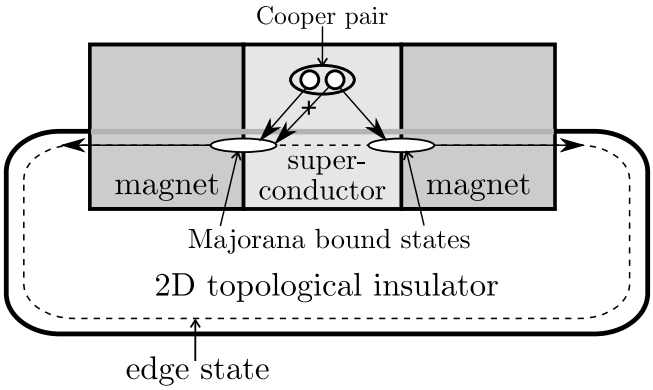

Figure 1.9: An edge of a two-dimensional topological insulator supports Majorana fermions when interrupted by ferromagnetic insulators and superconductors. Majorana fermions allow for only one electron out of a Cooper pair to exit at each side, acting as a perfect Cooper pair splitter.

Chapter 8: Electrically detected interferometry of Majorana fermions in a topological insulator

Chiral Majorana modes, one-dimensional analogue of Majorana bound states exist at a tri-junction of a topological insulator, s-wave superconductor, and a ferromagnetic insulator. Their detection is problematic since they have no charge. This is an obstacle to the realization of topological quantum computation, which relies on Majorana fermions to store qubits in a way which is insensitive to decoherence. We show how a pair of neutral Majorana modes can be converted reversibly into a charged Dirac mode. Our Dirac-Majorana converter, shown in Fig. 1.10, enables electrical detection of a qubit by an interferometric measurement.

Chapter 9: Domain wall in a chiral *p*-wave superconductor: a pathway for electrical current

Superconductors with $p_x \pm ip_y$ pairing symmetry are characterized by chiral edge states, but these are difficult to detect in equilibrium since the resulting magnetic field is screened by the Meissner effect. Nonequilibrium detection is hindered by the fact that the edge excitations are unpaired Majorana fermions, which cannot transport charge near the Fermi level. In this chapter we show that the boundary between $p_x + ip_y$ and $p_x - ip_y$ domains forms a one-way channel for electrical charge (see Fig. 1.11). We derive a product rule for the domain wall conductance, which allows to cancel the effect of a tunnel barrier between metal electrodes and superconductor and provides a unique signature of topological superconductors in the chiral p-wave symmetry class.

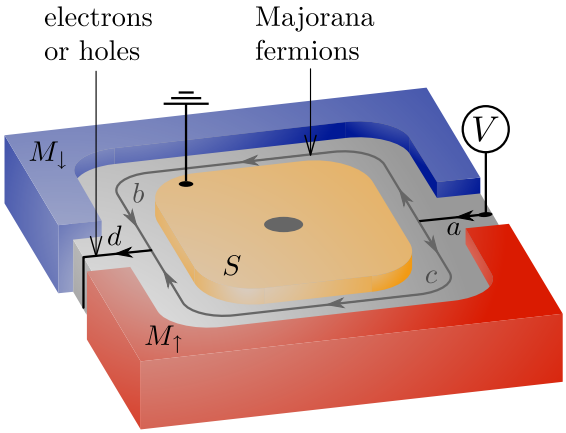

Figure 1.10: A Mach-Zehnder interferometer formed by a three-dimensional topological insulator (grey) in proximity to ferromagnets ($M_\uparrow$ and $M_\downarrow$) of opposite polarizations and a superconductor (S). Electrons approaching the superconductor from the magnetic domain wall are split into pairs of Majorana fermions, which later recombine into either electrones or holes.

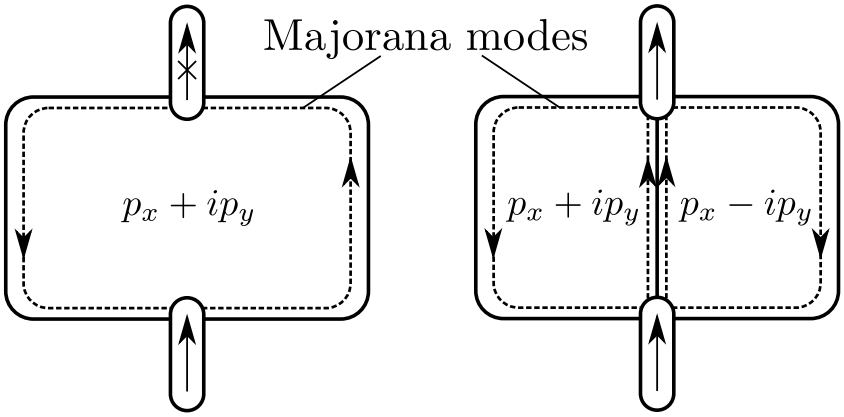

Figure 1.11: Left panel: a single chiral Majorana mode circling around a p-wave superconductor cannot carry electric current due to its charge neutrality. Right panel: when two chiral Majorana modes are brought into contact, they can carry electric current due to interference.

Chapter 10: Quantized conductance at the Majorana phase transition in a disordered superconducting wire

Superconducting wires without time-reversal and spin-rotation symmetries can be driven into a topological phase that supports Majorana bound states. Direct detection of these

zero-energy states is complicated by the proliferation of low-lying excitations in a disordered multi-mode wire. We show that the phase transition itself is signaled by a quantized thermal conductance and electrical shot noise power, irrespective of the degree of disorder. In a ring geometry, the phase transition is signaled by a period doubling of the magnetoconductance oscillations. These signatures directly follow from the identification of the sign of the determinant of the reflection matrix as a topological quantum number (as shown in Fig. 1.12).

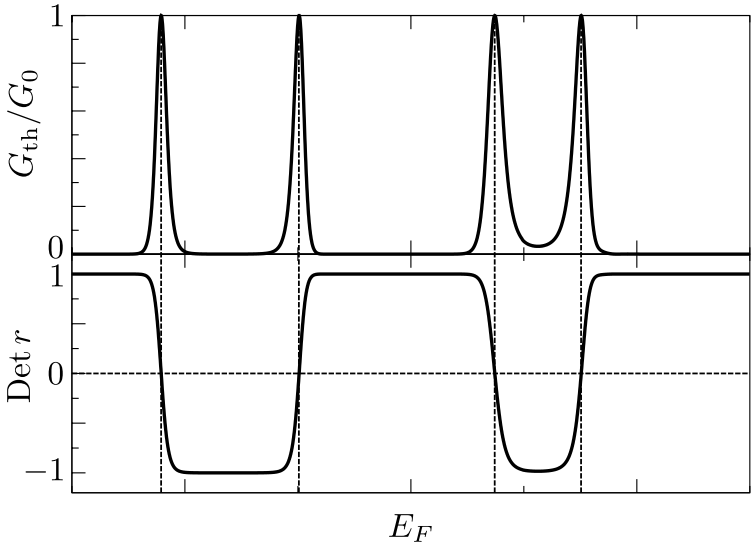

Figure 1.12: Thermal conductance (top panel) and the determinant of a reflection matrix (bottom panel) of a quasi one-dimensional superconducting wire as a function of Fermi energy. At the topological phase transitions (vertical dashed lines) the determinant of the reflection matrix changes sign, and the thermal conductance has a quantized spike.

Chapter 11: Theory of non-Abelian Fabry-Perot interferometry in topological insulators

Interferometry of non-Abelian edge excitations is a useful tool in topological quantum computing. In this chapter we present a theory of non-Abelian edge state interferometry in a 3D topological insulator brought in proximity to an s-wave superconductor. The non-Abelian edge excitations in this system have the same statistics as in the previously studied 5/2 fractional quantum Hall effect and chiral p-wave superconductors. There are however crucial differences between the setup we consider and these systems. The two types of edge excitations existing in these systems, the edge fermions ψ and the edge vortices σ, are charged in fractional quantum Hall system, and neutral in the topological insulator setup. This means that a converter between charged and neutral excitations,

shown in Fig. 1.13, is required. This difference manifests itself in a temperature scaling exponent of $-7/4$ for the conductance instead of $-3/2$ as in the 5/2 fractional quantum Hall effect.

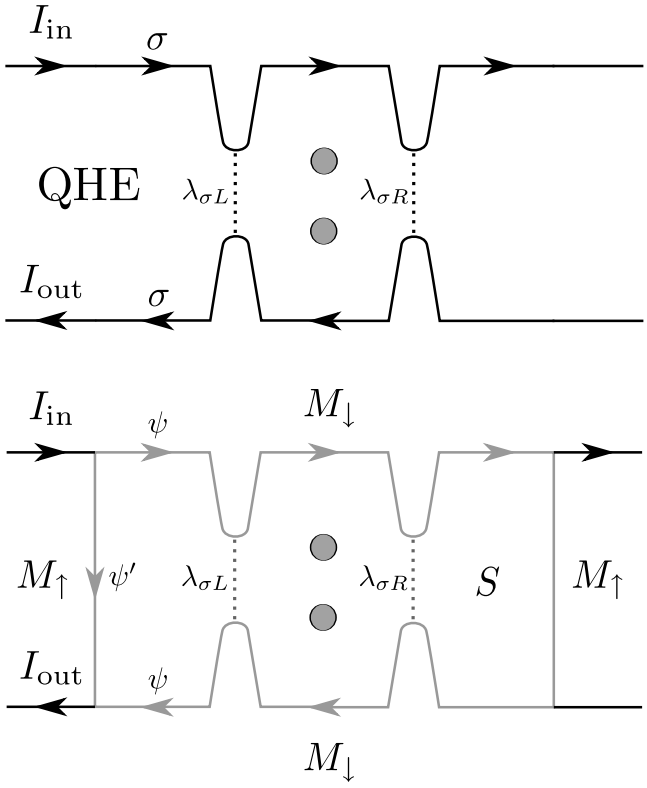

Figure 1.13: Top panel: non-Abelian Fabry-Perot interferometer in the 5/2 fractional quantum Hall effect. The electric current is due to tunneling of σ-excitations with charge $e/4$. Bottom panel: non-abelian Fabry-Perot interferometer in a topological insulator/superconductor/ferromagnet system. The electric current is due to fusion of two ψ-excitations at the exit of the interferometer.

Chapter 12: Probing Majorana edge states with a flux qubit

A pair of counter-propagating Majorana edge modes appears in chiral p-wave superconductors and in other superconducting systems belonging to the same universality class. These modes can be described by an Ising conformal field theory. We show how a superconducting flux qubit attached to such a system couples to the two chiral edge modes via the disorder field of the Ising model. Due to this coupling, measuring the back-action

of the edge states on the qubit allows to probe the properties of Majorana edge modes in the setup drawn in Fig. 1.14.

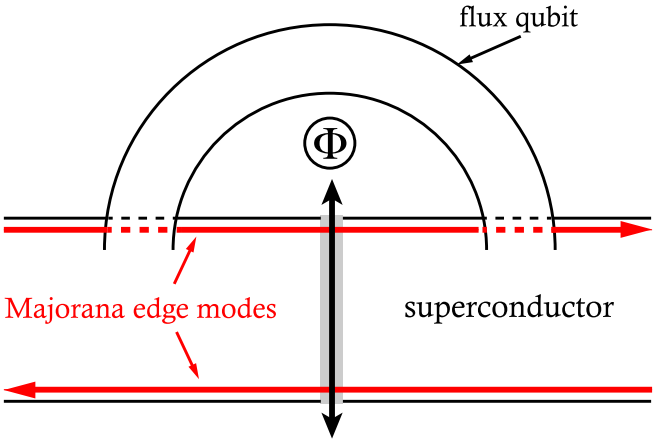

Figure 1.14: Schematic setup of the Majorana fermion edge modes coupled to a flux qubit. A pair of counter-propagating edge modes appears at two opposite edges of a topological superconductor. A flux qubit, consisting of a superconducting ring and a Josephson junction, shown as a gray rectangle, is attached to the superconductor in such a way that it does not interrupt the edge states' flow. As indicated by the arrow across the weak link, vortices can tunnel in and out of the superconducting ring through the Josephson junction.

Chapter 13: Anyonic interferometry without anyons: how a flux qubit can read out a topological qubit

Proposals to measure non-Abelian anyons in a superconductor by quantum interference of vortices suffer from the predominantly classical dynamics of the normal core of an Abrikosov vortex. We show how to avoid this obstruction using coreless Josephson vortices, for which the quantum dynamics has been demonstrated experimentally. The interferometer is a flux qubit in a Josephson junction circuit, which can nondestructively read out a topological qubit stored in a pair of anyons — even though the Josephson vortices themselves are not anyons. The flux qubit does not couple to intra-vortex excitations, thereby removing the dominant restriction on the operating temperature of anyonic interferometry in superconductors. The setup of Fig. 1.15 allows then to create and manipulate a register of topological qubits.

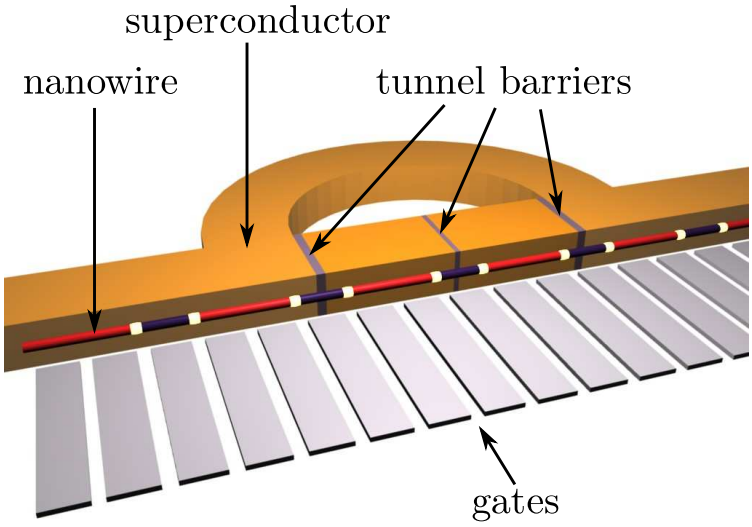

Figure 1.15: Register of topological qubits, read out by a flux qubit in a superconducting ring. The topological qubit is encoded in a pair of Majorana bound states (white dots) at the interface between a topologically trivial (blue) and a topologically nontrivial (red) section of an InAs wire. The flux qubit is encoded in the clockwise or counterclockwise persistent current in the ring. Gate electrodes (grey) can be used to move the Majorana bound states along the wire.